International Journal of Heat and Mass Transfer 51 (2008) 6157–6168

Contents lists available at ScienceDirect

International Journal of Heat and Mass Transfer

journal homepage: www.elsevier.com/locate/ijhmt

3D conjugate heat transfer with thermal radiation in a hollow cube exposed to external flow

C. Albanakis, D. Bouris *

Department of Engineering and Management of Energy Resources, University of Western Macedonia, Bakola and Sialvera, 50100 Kozani, Greece

ARTICLE INFO

Article history:
Received 23 July 2007
Available online 24 May 2008

Keywords:
3D RANS
Conjugate heat transfer
Thermal radiation
Cube envelope

ABSTRACT

The interaction of an asymmetrically heated cube envelope exposed to turbulent external flow is numerically studied using a three dimensional computational fluid dynamics control volume approach with conjugate heat transfer, including thermal radiation effects. An analytical approach is used for thermal radiation modelling with an implicit boundary condition for convective and radiative heat transfer at solid–fluid interfaces. For external flow Reynolds numbers of 2×10^5–10^6 and heat flux values of $q = 20, 40\ \mathrm{W\ m^{-2}}$, a weak but turbulent ($Ra = 1.5$–$5 \times 10^9$) buoyant flow is induced inside the cube. The temperature distribution of the inner surfaces is significantly affected by heat flux orientation with regard to external flow as well as the relative influence of convective and thermal radiation heat transfer.

1. Introduction

Natural convection is found in a number of applications such as electronics, aeronautics, building engineering, solar energy collectors, aerospace systems, etc, where forced convection and thermal radiation might also be present. Buoyant flows in indoor spaces have been receiving much attention recently and understanding the mechanisms that link them with external wind flow is valuable information for natural or hybrid ventilation applications [1]. An interesting situation arises when a building is subject to external airflow while simultaneously exposed to solar radiation since it combines a number of heat transfer modes: natural and forced convection, thermal radiation and conduction through the envelope. The purpose of the present study is to present a numerical methodology that is being developed to study the fundamental 3D configuration, for all involved heat transfer modes.

Turbulent flow and heat transfer past a surface mounted cube has been the subject of both experimental and numerical studies. Meinders et al. [2] and Nakamura et al. [3] performed experimental measurements of the local and mean Nusselt number distribution on the surfaces of a heated cube exposed to turbulent external flow and the latter developed correlations for the external surface heat transfer as a function of Reynolds number. The inside of the cube was solid and at steady heating conditions. Meinders and Hanjalic [4] extended these studies to heat transfer from two surface mounted cubes, finding that the distribution of the heat transfer coefficient depends on the vortex shedding of the upstream cube but that the average value remains independent of the relative placement of the two cubes. Turbulent flow past a surface mounted cube has been a challenging problem for numerical studies due to the complex flow pattern that includes recirculation regions, stagnation points and unsteady vortex shedding. Cheng et al. [5] compared large eddy simulations to standard Reynolds averaged modelling using the k–ε model and Tsuchiya et al. [6] investigated the applicability of modifications to the standard k–ε model for bluff body flows where excessive turbulence energy production is usually predicted in the stagnation regions. Iaccarino et al. [7] and Rodi [8] attribute the superior predictions of LES for this type of flow to correct modelling of both turbulence energy production and vortex shedding. Unfortunately, since the computational cost of this type of simulation is high and even unsteady RANS are overwhelming for parametric studies [7], some of the inaccuracies of RANS models must still be tolerated [8] although knowledge of the shortcomings is important for extracting dependable conclusions.

In a differentially heated cubic enclosure, natural convection dominates and this has also been a subject of interest for many years. Markatos et al. [9] numerically studied the buoyant flow of smoke in a square enclosure and the numerical modelling of the buoyancy forces in gases is still being refined [10]. A common configuration for natural convection in enclosures is when one side of the enclosure (usually a cube) is heated and the opposite side is cooled. The laminar flow experiment by Bajorek and Lloyd [11], which involved a 2D enclosure with obstacles (baffles) extending from the top and bottom walls, has been used as a validation test case for both enclosure natural convection and conjugate heat transfer [12]. Tian and Karayiannis [13] experimentally studied a 2D enclosure with differentially heated side walls, but for a moderately turbulent flow ($Ra \sim 10^9$), without obstacles. Dol and Hanjalic

* Corresponding author. Tel.: +30 24610 56675.
E-mail address: dmpouris@uowm.gr (D. Bouris).

0017-9310/$ - see front matter © 2008 Elsevier Ltd. All rights reserved.
doi:10.1016/j.ijheatmasstransfer.2008.01.038

Nomenclature

A	surface area, m^2
C_p	specific heat, J kg^{-1} K^{-1}
C_μ, C_1, C_2, C_3	k–ε model constants
d, L, H	geometric dimensions of configurations, m
dn	normal distance from solid surface, m
e	emissivity
F_t	interpolation coefficient
F_{ij}	view factor between surface i and j
g	acceleration of gravity, m s^{-2}
Gr	Grasshoff number, $\beta g H^3(T_h - T_c)/\nu^2$
h	convective heat transfer coefficient, W m^{-2} K^{-1}
$h_{ri,j}$	linearised radiative heat transfer coefficient for surfaces i and j, W m^{-2} K^{-1}
k_t	thermal conductivity, W m^{-1} K^{-1}
k	turbulence kinetic energy, m^2 s^{-2}
Nu	convective Nusselt number, hL/k_t
P	pressure, Pa
P_k, G_k	turbulence kinetic energy production terms, kg m^{-1} s^{-3}
q	heat flux, W m^{-2}
$q_{j,i}$	radiative heat flux between surfaces i and j, W m^{-2}
q_r	radiative heat flux term, W m^{-2}
Ra	Rayleigh number, $g\beta(T_h - T_c)H^3/\nu\alpha$
Re	Reynolds number, $U_0 H/\nu$
S_T	source term in energy equation, W m^{-3}
T	temperature, K
T_o	reference temperature for buoyancy force calculation, K
u	velocity, m s^{-1}
x, y, z	Cartesian directions

Greek symbols

α	thermal diffusivity, m^2 s^{-1}
β	thermal expansion coefficient, K^{-1}
ε	turbulence energy dissipation rate, m^2 s^{-3}
ΔT	temperature difference, K
η, ξ	secondary Cartesian directions in Fig. 1
μ, μ_t, μ_{eff}	dynamic, turbulent and effective viscosity, kg m^{-1} s^{-1}
ν	kinematic viscosity, m^2 s^{-1}
ρ	density, kg m^{-3}
σ	Stefan–Boltzmann constant (5.67×10^{-8} W m^{-2} K^{-4})
σ_T	turbulent Prandtl number

Subscripts

i = 1, 2, 3	Cartesian notation corresponding to x, y, z directions, respectively
sf	solid–fluid interface
s	solid
f	fluid
c	cold wall
h	hot wall
o	upstream flow

[14] performed numerical studies of turbulent natural convection in a side-heated enclosure with a number of turbulence models and found that the low-Reynolds number k–ε model variants fail to represent details of the flow but are capable of providing qualitative information. Radiation effects in these configurations can become important for large temperature differences, or when convection is not prominent and Kasemi and Naraghi [15] performed 2D numerical studies of the laminar flow in a differentially side heated square enclosure at low values of gravitational acceleration. The effects of radiation were modelled using the discrete exchange factor method and became more important as convection was reduced at low-g. Mezrhab et al. [16] used the radiosity approach to include radiation effects in their study of 2D laminar natural convection in a cavity with a square body at its center and more recently Dharma Rao et al. [17] used an ADI solver to perform a detailed conjugate heat transfer analysis of 2D conduction, natural convection and radiative heat transfer in a horizontal fin array considered as a two-fin enclosure. Sharma et al. [18] studied turbulent flow in a differentially heated square enclosure with thin walls, for which conjugate heat transfer of convection and conduction was considered at the interface but the walls themselves were modelled as one dimensional fins. The presence of three dimensional solid objects was considered by Consalvi et al. [19] who presented a methodology for solving turbulent flow and heat transfer in enclosures under conditions of fire. Sharma et al. [18] and Consalvi et al. [19], used the k–ε model for turbulence effects, the radiosity method for radiation and the harmonic mean of the solid and fluid thermal conductivities was used at the interface. However, Chen and Han [20], who focused on modelling conjugate heat transfer with SIMPLE based algorithms, found that the application of the harmonic mean across the interface might lead to erroneous solutions.

There are a number of complex physical phenomena present in both the flow past a surface mounted cube and in the buoyant flow inside a differentially heated cubic enclosure that have been addressed separately in the past, as shown in the preceding discussion, but the combined configuration has not received much attention. Bouris [21] and Petridou and Bouris [22] have previously performed studies of the flow and heat transfer past a hollow surface mounted cube, examining both the effects of turbulence modelling assumptions as well as the variation of the thermal fields through the cube envelope. However, radiation effects were not included in the study and thermal sources were uniformly distributed inside the cube. In the present study, a numerical methodology is presented that allows for the simultaneous solution of forced and buoyant turbulent flow with conjugate convective, conductive and radiative heat transfer through solid–fluid interfaces. Special attention is placed on the thermal boundary condition at the solid–fluid interface so that it is implicitly included in the solution rather than through a separate iterative procedure.

2. Numerical methodology

2.1. Flow field

The numerical method is based on the Reynolds averaged Navier–Stokes equations (RANS) with the mass, momentum (velocities: u_1, u_2, u_3, pressure: P) and enthalpy (C_p: specific heat, T: temperature) equations written in Cartesian notation (i = 1, 2, 3 correspond to x, y, z directions, respectively):

$$\frac{\partial}{\partial x_i}(\rho u_i) = 0 \tag{1}$$

$$\frac{\partial}{\partial x_j}(\rho u_j u_i) = -\frac{\partial P}{\partial x_i} + \frac{\partial}{\partial x_j}\left[\mu_{eff}\left(\frac{\partial u_i}{\partial x_j} + \frac{\partial u_j}{\partial x_i}\right)\right] + \rho\beta g_i(T - T_o) \tag{2}$$

$$\frac{\partial}{\partial x_j}(\rho u_j C_P T) = \frac{\partial}{\partial x_j}\left[\left(k_t + \frac{\mu_t C_P}{\sigma_T}\right)\frac{\partial T}{\partial x_j}\right] + S_T \tag{3}$$

where k_t is the thermal conductivity, ρ the density, μ the dynamic viscosity, β the thermal expansion coefficient and g_i is the acceleration of gravity ($g_1 = g_3 = 0$, $g_2 = 9.81$ m s^{-2}) with T_o the reference temperature for buoyancy force calculation. This system of equations applies to the whole domain whether fluid or solid (velocities become zero), dominated by natural or forced convection (the

buoyancy term becomes negligible in areas of no temperature difference) and it is solved on a Cartesian grid with a collocated variable arrangement using the SIMPLE pressure correlation algorithm [23] with corrections for the cell face velocities [24]. For calculation of the turbulent viscosity (μ_t):

$$\mu_{\text{eff}} = \mu + \mu_t = \mu + C_\mu \frac{k^2}{\varepsilon} \tag{4}$$

the transport equations for turbulent kinetic energy (k) and turbulent energy dissipation (ε) are:

$$\frac{\partial}{\partial x_j}(\rho u_j k) = \frac{\partial}{\partial x_j}\left[\mu_{\text{eff}} \frac{\partial k}{\partial x_j}\right] + P_k + G_k - \rho\varepsilon \tag{5}$$

$$\frac{\partial}{\partial x_j}(\rho u_j \varepsilon) = \frac{\partial}{\partial x_j}\left[\mu_{\text{eff}} \frac{\partial \varepsilon}{\partial x_j}\right] + [C_1(P_k + C_3 G_k) - C_2\varepsilon]\frac{\varepsilon}{k} \tag{6}$$

$$P_k = \mu_t\left(\frac{\partial u_i}{\partial x_j} + \frac{\partial u_j}{\partial x_i}\right)\frac{\partial u_i}{\partial x_j}, \quad G_k = -\frac{\mu_t}{\sigma_T} g_i \beta \frac{\partial T}{\partial x_i} \tag{7}$$

The constants in (3)–(7) are $C_\mu = 0.09$, $C_1 = 1.44$, $C_2 = 1.92$, $\sigma_T = 1.0$, $\sigma_k = 1.0$, $\sigma_\varepsilon = 1.3$. Test calculations using $C_3 = \tanh(u_2/(u_1^2 + u_3^2)^{0.5})$, as used by Sharma et al. [18], did not show any significant differences compared to the suggestion of Markatos et al. [9] that it is acceptable to take the buoyancy constant C_3 to be zero for enclosures – possibly because of the low (only moderately turbulent) Rayleigh number of the flows considered. The k–ε turbulence model was used [25–27] but it is important to mention that although the best results for turbulent heat transfer with the k–ε model are obtained with its low-Reynolds number variants [28], these are very demanding in terms of grid density near the walls and convergence stability so the standard wall function approach has been used here. Buoyancy forces were calculated based on density differences arising from temperature variations with respect to a reference temperature-density value. This is based on the commonly used Boussinesq approximation that has recently been re-examined by Sparrow and Abraham [10], who concluded that, as long as the fluid properties and reference density are considered at the mean surrounding temperature, it is acceptably accurate compared to the computationally expensive alternative of directly inserting the buoyancy term. All terms are discretised using second order differences while second order upwind differencing of the convective terms was implemented using the fully bounded second order BSOU scheme [29].

2.2. Radiative heat transfer

The last term in (3) is a heat source term that can be added to the temperature equation to represent the effects of heat sources, such as thermal radiation. First, a finite number of surfaces (N) are chosen as a radiative heat transfer system. In the present study, these are the solid surface control volume cell faces that surround the enclosure and are determined by the grid resolution. Calculation of the net radiative heat fluxes between these surfaces could be calculated using the commonly applied radiosity approach, which however requires a matrix inversion that may become excessively demanding for a large number of surfaces. Here, thermal radiation between solid surfaces separated by a non-participating medium (air) is modelled according to an analytical approach proposed by Clarke [30] that involves simpler calculations. The emissive power (q_i) from any surface of area (A_i), emissivity (e_i) and temperature (T_i) is

$$q_i = e_i \cdot \sigma \cdot A_i \cdot T_i^4 \tag{8}$$

with (σ) the Stefan–Boltzman constant. This will be distributed among all other surfaces in an enclosure, depending on the view factor between surface pairs (F_{ij}), and will be absorbed or reflected by them, possibly returning to the original surface or escaping through openings in the enclosure. The reflected radiation depends on the emissivity of the surfaces but for the most common surfaces found in building enclosures the emissivity is high (>0.8), leading to a limited number of reflections. Based on this observation, an analytic solution can be derived, that considers reflected radiation between surface pairs, including reflections from a third participating surface i.e. direct and indirect radiation resulting from one intermediate reflection. The heat flux being absorbed at surface 2 that originates at surface 1 or results from infinite reflections between the two surfaces or any other single intermediate surface (n) is given as a geometrical progression:

$$\begin{aligned} q_{(n)1\to 2} &= e_2(1-e_n)e_1\sigma A_1 T_1^4 F_{1\to n}F_{n\to 2} + e_2(1-e_1)(1-e_2) \\ &\quad \times (1-e_n)^2 e_1 \sigma A_1 T_1^4 F_{1\to n}^2 F_{n\to 2}^2 F_{2\to 1} + \cdots \infty \\ &= \frac{e_2(1-e_n)e_1\sigma A_1 T_1^4 F_{1\to n}F_{n\to 2}}{1-(1-e_1)(1-e_2)(1-e_n)F_{1\to n}F_{n\to 2}F_{2\to 1}} \end{aligned} \tag{9}$$

so the flux arriving at 2 from 1, through any other surface, would be calculated as the sum of (9) for all surfaces $n = 1, N$ (except 1 and 2). The total radiation exchange between surface ($i = 1$) and surface ($j = 2$) can be linearised in the form

$$q_{j,i} = q_{2,1} = h_{r2,1} \cdot A_1 \cdot (T_2 - T_1) \tag{10}$$

where $h_{r2,1}$ is the linearised radiative heat transfer coefficient that can be calculated from the infinite geometrical progression of three-surface interactions (9) and is [30]:

$$\begin{aligned} h_{r2,1} &= (T_2^2 + T_1^2)\cdot(T_2 + T_1) \\ &\quad \cdot \left\{ \frac{e_1 \cdot e_2 \cdot F_{1\to 2}}{\left[1-(1-e_1)\cdot(1-e_2)\cdot F_{1\to 2}^2 A_1/A_2\right]} + e_1 \cdot e_2 \cdot \sigma \cdot A_2 \right. \\ &\quad \left. \times \sum_{i=3}^{N} \frac{(1-e_1)\cdot F_{1\to i}F_{2\to i}}{A_i \cdot [1-(1-e_1)\cdot(1-e_2)\cdot(1-e_i)\cdot F_{1\to i}F_{i\to 2}F_{2\to 1}]} \right\} \end{aligned} \tag{11}$$

In (11), the view factor reciprocity relation $F_{2\to 1} = F_{1\to 2}A_1/A_2$ has been taken into account and summation refers to all of the remaining surfaces (other than the surface pair being considered) involved in radiation exchange. Net radiation for any surface (i) is calculated from the sum $\left(\sum_{j=1,N-1} q_{j,i}\right)$ where $q_{1,2} = -q_{2,1}$ and $h_{r1,2} = h_{r2,1}A_1/A_2$, so that for all surface pairs being considered, only half of the heat transfer rates (q) need to be calculated. The term in brackets in (11) involves computationally expensive summation for all surfaces but, since it is only geometric and hence temperature independent, it can be calculated once at the beginning of the calculation procedure and then the expression for $h_{rj,i}$ is easily updated depending on the local surface temperatures before being inserted in the source terms in (3). Calculation of the view factors (F_{ij}) in (11) is facilitated by the use of the Cartesian grid and can be based on the analytical expressions given by Howell [31] (see Fig. 1 for notation):

$$F_{1-2} = \frac{1}{(x_2 - x_1)\cdot(y_2 - y_1)} \sum_{l=1}^{2}\sum_{k=1}^{2}\sum_{j=1}^{2}\sum_{i=1}^{2}(-1)^{(i+j+k+l)} G(x_i, y_j, \eta_k, \xi_l) \tag{12}$$

where G is given for parallel surfaces

$$\begin{aligned} G = \frac{1}{2\pi}\cdot\left\{ (y-\eta)\cdot\sqrt{(x-\xi)^2+z^2}\cdot\tan^{-1}\left[\frac{y-\eta}{\sqrt{(y-\eta)^2+z^2}}\right]\right. \\ + (x-\xi)\cdot\sqrt{(y-\eta)^2+z^2}\cdot\tan^{-1}\left[\frac{x-\xi}{\sqrt{(y-\eta)^2+z^2}}\right] \\ \left. - \frac{z^2}{2}\cdot\ln[(x-\xi)^2+(y-\eta)^2+z^2]\right\} \end{aligned} \tag{13}$$

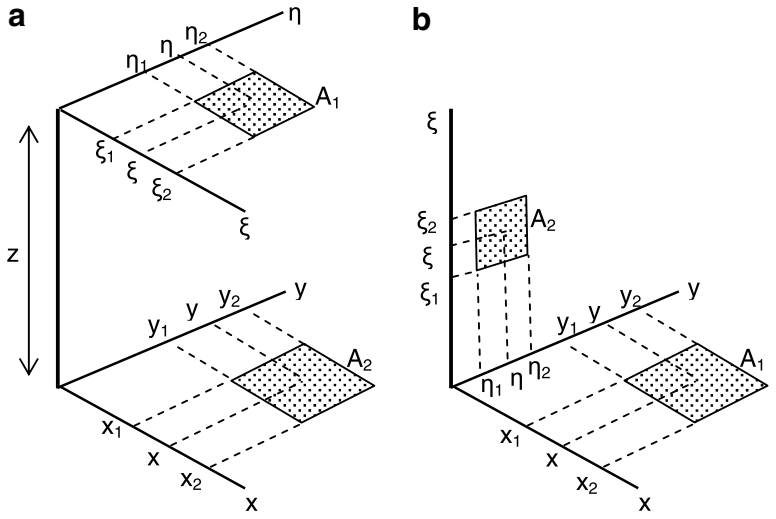

Fig. 1. Notation for calculation of view factors in (12)–(14): (a) parallel surfaces; (b) perpendicular surfaces.

and perpendicular surfaces:

$$G=\frac{1}{2\pi}\cdot\left\{(y-\eta)\cdot\sqrt{x^2+\xi^2}\cdot\tan^{-1}\left[\frac{(y-\eta)}{\sqrt{x^2+\xi^2}}\right]-\frac{1}{4}\cdot[x^2+\xi^2-(y-\eta)^2]\cdot\ln[x^2+\xi^2+(y-\eta)^2]\right\} \tag{14}$$

As already mentioned, (11) does not take into account radiation that might have reached the surface after more than one reflection (i.e. four or more participating surfaces). For situations with low emissivity surfaces, this could lead to errors in the calculated radiative heat transfer so a numerical check is performed at the end of the procedure in order to verify that the total radiative energy leaving any surface is equal to that given by (8). Deviations were insignificant in the present study (<10^{-5}%) but, when present, they can be overcome by distributing the remaining energy among all the surfaces, on a view factor weighted basis. A similar procedure is performed to verify that the summation of view factors for any surface equals unity, deviations (here, <10^{-7}%) to which must be attributed only to numerical errors since there are no assumptions in the methodology.

The view factors can also be exploited to implement shading between any two surfaces (A) and (B) using the following procedure: (a) the view factor is calculated according to (12)–(14) but only if the angles between the surface direction vectors ($\vec{n}_A, \vec{n}_B$) and the line segment joining the surface centers ($\overline{AB}$) are both <90°. If not, then the surfaces are not facing each other and the view factor is set to zero; (b) the surface pair (A, B) is examined with relation to the remaining surfaces in the system ($i = 3, N$) and an obstructing (shading) surface is determined when only one of F_{Ai}, F_{Bi} is non-zero and the intercept point between the surface (i) and the line segment ($\overline{AB}$) is between the two surfaces and within the limits of surface (i). Finding these co-ordinates is based on basic 3D vector analysis. If an obstructing surface is found then $F_{AB} = 0$ but (11) must still be used since there will be indirect radiation exchange between the surfaces.

For inclusion of radiation effects in the calculation and consideration of heat flow through solid–fluid interfaces, a conjugate heat transfer boundary condition must be applied at all solid–fluid interfaces and the enthalpy equation must be solved in both fluid and solid domains, the only difference being in the velocities (zero for solid domain) and the diffusion coefficients appearing in (3). Here, for implementation of the conjugate heat transfer boundary condition, an implicit procedure is introduced. At any solid–fluid interface, the heat balance requires that:

$$A\cdot\left(k_t\frac{\partial T}{\partial n}\right)_{\text{solid}}=A\cdot\left(k_t\frac{\partial T}{\partial n}\right)_{\text{fluid}}+q_r \tag{15}$$

where q_r is the radiation term calculated from the contribution of all surfaces, according to (11). An assumption is made that the interface temperature (T_{sf}) will be a linear function of the solid and fluid temperatures neighbouring the interface:

$$T_{sf}=F_t\cdot T_s+(1-F_t)\cdot T_f \tag{16}$$

It will subsequently be shown that it is in fact not linear but the initial hypothesis facilitates analysis, without loss of generality. Substitution of (16) into (15) leads to

$$F_t=\frac{1}{k_{ts}/dn_{sf-s}+k_{tf}/dn_{f-sf}}\cdot\left[\frac{k_{ts}}{dn_{sf-s}}-\frac{q_r}{A(T_s-T_f)}\right] \tag{17}$$

and (16) is rewritten as:

$$T_{sf}=\frac{\left(\frac{k_{ts}}{dn_{sf-s}}T_s+\frac{k_{tf}}{dn_{f-sf}}T_f\right)A-q_r}{(k_{ts}/dn_{sf-s}+k_{tf}/dn_{f-sf})A} \tag{18}$$

where (k_{ts}, k_{tf}) are the solid and fluid thermal conductivities respectively, (A) is the surface area of the control volume cell faces that neighbour the interface and (dn_{f-sf}, dn_{sf-s}) are the normal distances between the control volume cell center and the interface on the fluid and solid side respectively. Notice that the interpolation parameter (F_t) is a function of the temperatures neighbouring the interface and the radiation heat flux. (18) is used for calculation of the surface temperatures appearing in (10) and (11) while for the discretisation of the enthalpy equation radiation is included as a source term for the solid side control volume and the following, equivalent but numerically more stable, condition is applied:

$$\left(k_t\frac{T'_{sf}-T_s}{dn}\right)_s=\left(k_t\frac{T_f-T'_{sf}}{dn}\right)_f,\quad T'_{sf}=\frac{k_{ts}/dn_{sf-s}\cdot T_s+k_{tf}/dn_{f-sf}\cdot T_f}{k_{ts}/dn_{sf-s}+k_{tf}/dn_{f-sf}} \tag{19}$$

where T'_{sf} is the surface temperature that would arise if (15) were applied without radiation effects i.e. the purely conductive boundary condition appearing in conjugate heat transfer without radiation [32]. In fact, this approach is very similar to that of Li and Durbetaki [33] and Consalvi et al. [19], except they both used a harmonic mean value for the thermal conductivity instead of calculating the surface temperature as is done here. Using the harmonic mean of (k_t/C_p) on

the fluid and solid side is a potential source of error in many steady state applications according to Chen and Han [20] and the present methodology avoids this problem.

The procedure of including conjugate heat transfer with radiation effects can be summarised as:

(a) calculation of the radiation term (q_r) depending on the wall surface (not cell center) temperatures that appear in (10). These are calculated through (18) based on values from the previous iteration.
(b) (q_r) is inserted as an energy equation source term (S_T) in (3) for the control volume on the solid side of the interface.
(c) implementation of (19) is achieved by using (T'_{sf}) for calculating the normal diffusion terms of both solid and fluid control volumes neighbouring the interface. Wall functions for turbulent boundary layers can be included in the usual manner, as presented for non-radiative conjugate heat transfer in [32].

Updating of the radiation heat fluxes is performed at every iteration of the SIMPLE solution procedure and interface temperatures are updated accordingly. The implementation has proven to be robust although some underrelaxation for the enthalpy equation was found beneficial. In the present approach, a single grid spans fluid and solid domains and the conjugate heat transfer boundary condition, including radiative effects, is implicitly applied in the solution of the system of equations. This is facilitated by the assumption of (16) and only the temperatures and heat flux required for the (F_t) coefficients are lagged in the iterative process.

3. Results

The numerical procedure was first validated through the simulation of relevant configurations in the published literature and then applied to parametrically study the situation of a hollow cube exposed to external fluid flow and a constant heat flux on one of its external surfaces.

For the flow inside the enclosure, validation was first performed for low-Rayleigh number flows in side heated enclosures, with and without radiation and internal obstacles, and then for a moderately high Rayleigh number flow. For the effect of the external flow on the cube envelope, the most common approach is to set a constant heat transfer coefficient on the external walls (e.g. [18]). Here, the turbulent flow past a surface mounted cube is calculated leading to local values of convective heat transfer on the external walls. For calculation of turbulent flow past a surface mounted cube, eddy viscosity models, such as the k–ε model applied here, admittedly lead to inaccuracies that are difficult to overcome but although variants to the model have been suggested their effectiveness is still questionable [8,5,22]. Large eddy simulations and even unsteady RANS have proven to yield the best results when compared to experiments but the computational cost is much higher. To the authors' knowledge, similar analysis of the heat transfer from a surface mounted cube has not been published but a previous attempt to examine it [22] indicated that similar conclusions should be drawn. Since the purpose here is to provide a more accurate estimation of the external wall heat transfer rather than applying a uniform constant value, and due to the excessive computational requirements for a better approach, the standard k–ε model was used but the accuracy of the calculation will be kept in mind and its effect on the results and conclusions will be discussed.

3.1. Isolated cubical enclosure

Bajorek and Lloyd [11] measured the flow and temperature field in a two dimensional square enclosure ($L \times L$) with two baffles ($d/L = 0.1$, $H/L = 0.25$) protruding from the middle of the top and bottom walls. The side walls were maintained at a constant temperature difference of ~15.5 K, leading to a Rayleigh number of $Ra = 3.5 \times 10^5$. Zimmerman and Acharya [12] studied this configuration numerically and found an important influence of the perfectly conducting wall boundary condition, as opposed to the more commonly used adiabatic one. In the present study, the configuration was extended by $3L$ in the third direction and discretised with a $50 \times 58 \times 21$ Cartesian grid. As expected, no 3D effects were observed. There were three grid cells defining the $0.1L$ thick top and bottom walls, which were assumed to have the thermal conductivity of the experimentally used plexiglass ($k_t = 0.665$ W m^{-1} K^{-1}). The same material was considered for the two baffles of the enclosure. The calculated flow and temperature field is presented in Fig. 2 with conjugate heat transfer considered for the baffles and the top and bottom walls. The favourable comparison with the experimental measurements of Bajorek and Lloyd [11] and the numerical predictions of Zimmerman and Acharya [12] is evident in Fig. 3. Inclusion of radiation effects (not shown) did not lead to any discernible differences, also in agreement with the findings of Zimmerman and Acharya [12], most probably because of the relatively small temperature differences and the constant temperature walls.

Radiation effects were examined by comparison with the numerical calculations of Kasemi and Naraghi [15] who used the discrete exchange factor method to calculate radiative heat transfer in a square ($H \times H$) enclosure for normal and low levels of gravitational acceleration. The advantage of this type of validation is that radiation effects and natural convection effects can be considered separately. A $22 \times 28 \times 15$ cartesian grid was used, with the depth direction exhibiting no 3D effects. As before, the top and bottom walls were discretised using three grid cells but assuming negligible thermal conductivity in order to simulate adiabatic boundary conditions. Results are presented in Fig. 4 for $H = 0.021$ m, a Grasshoff number of $Gr = 700$, and cold–hot wall temperature ratio of $T_c/T_h = 0.5$. Radiation effects are initially omitted, leading to an almost conductive, linear, behavior, where the weak natural convection plays a negligible role. With radiation present, natural convection remains at low levels but the temperature distribution along the hot and cold walls is significantly altered. Agreement

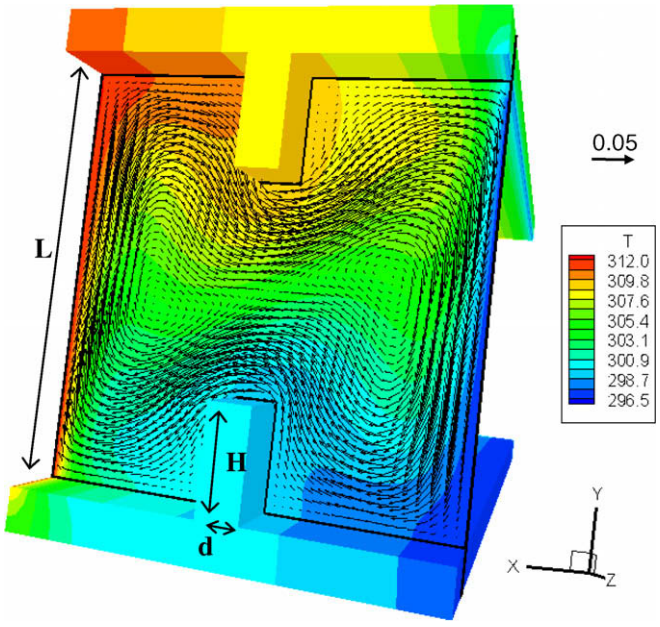

Fig. 2. Flow field vectors (m/s) and temperature field contours (K) for buoyant flow in an enclosure with two baffles ($Ra = 3.5 \times 10^5$).

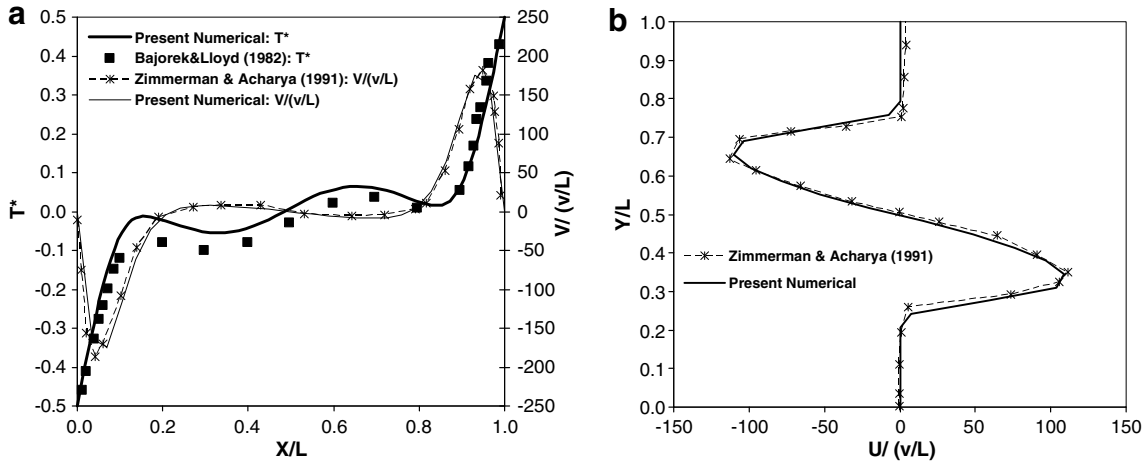

Fig. 3. Comparison with experimental and numerical results: (a) for the non-dimensional form $T^* = [T - (T_h + T_c)/2]/(T_h - T_c)$ and $V/(v/L)$ along the centreline between the hot and cold wall; (b) $U/(v/L)$ vertically, midway between the hot and cold wall.

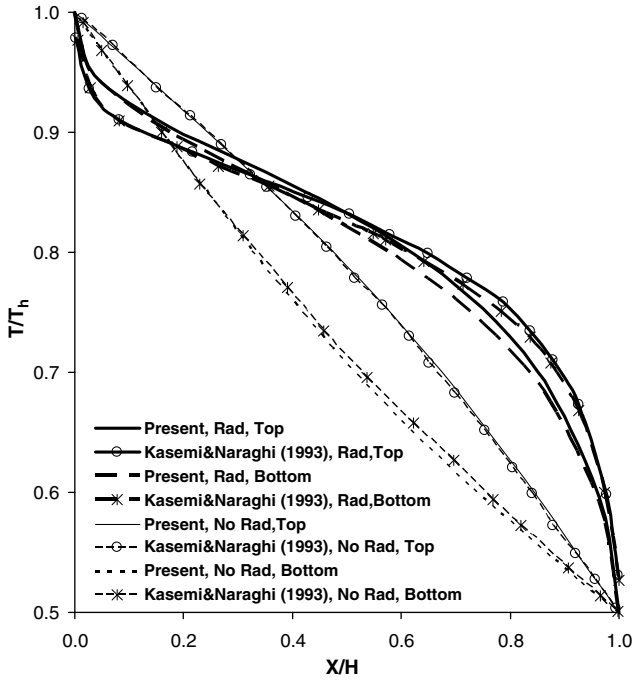

Fig. 4. Temperature distribution between hot and cold walls along top and bottom walls, with and without radiation effects.

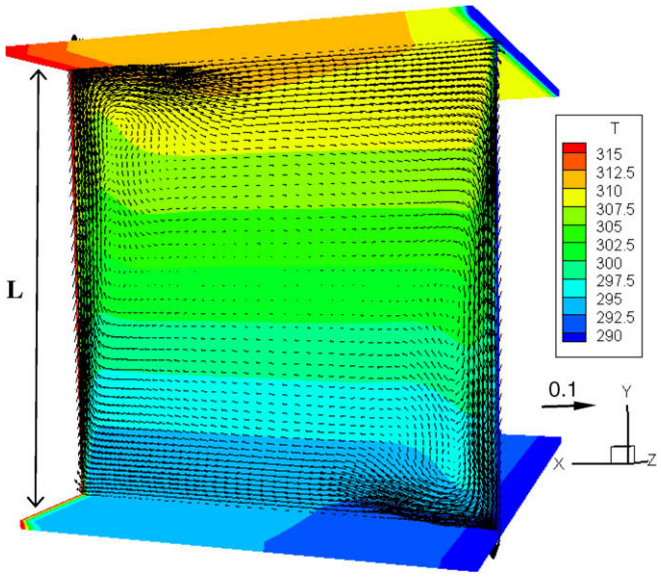

Fig. 5. Flow field vectors (m s^{-1}) and temperature field contours (K) for buoyant flow in an enclosure ($Ra = 1.58 \times 10^9$).

with the results of Kasemi and Naraghi [15] is considered acceptable since differences are below ~5% of $(T_h - T_c)$.

Turbulent flow in a square $(L \times L)$ enclosure with hot (T_h) and cold (T_c) opposite vertical walls has been examined by comparison with the results of Tian and Karayiannis [13]. The dimensions of their experimental configuration have been retained in all directions ($2L$ in the third direction) and the calculated flow field is presented in Fig. 5. This is a moderately turbulent Rayleigh number flow ($Ra = 1.58 \times 10^9$), turbulence onset being at roughly 10^8, but still poses a challenging numerical exercise. Results with a 32^3 grid, clustered near the walls, are presented in Figs. 6 and 7 for temperature and velocity fields, respectively. Agreement is generally acceptable and calculations with a 62^3 grid did not show significant improvements. According to Tian and Karayiannis [13], the mean Nusselt number along the wall should be $Nu = 64$ and the present calculations gave a 15% difference for both the 32^3 and 62^3 grids so the representation of the general features of the flow is considered acceptable for the purpose of the study. Sharma et al. [18] reached similar conclusions for grids ranging from 42×42 to 82×82 for higher Rayleigh numbers ($Ra \sim 10^{10}$) even though they did not apply any type of wall boundary approximation such as wall functions or a low-Reynolds number variant of the k–ε model.

3.2. Hollow cube subject to external heating and flow

The chosen configuration is that of a hollow cube exposed to an external flow of cool air and simultaneously subjected to a heat flux on one of its external sides. The enclosure dimensions are $3 \times 3 \times 3$ m with 0.2 m thick walls and $k_t = 0.14$ W m^{-1} K^{-1}, $\rho = 2300$ kg m^{-3}, $C_p = 650$ J kg^{-1} K^{-1}, $e = 0.9$. This gives emissivity and a thermal permeability factor (0.7 W m^{-2} K^{-1}) corresponding to characteristic building materials. The computational domain extends $4H$ above the cube, $6H$ in the spanwise direction and $12H$ in the flow direction with the cube $3.5H$ from the inlet boundary. The upstream flow velocity was uniform and the temperature constant

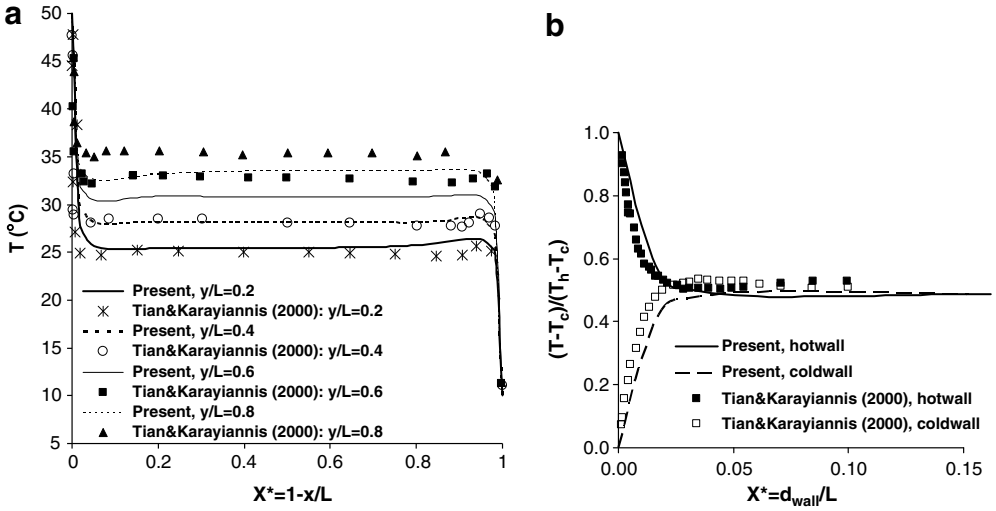

Fig. 6. (a) Temperature profiles between hot and cold walls at various heights of the enclosure. (b) Temperature boundary layer near the hot and cold wall at $y/L = 0.5$.

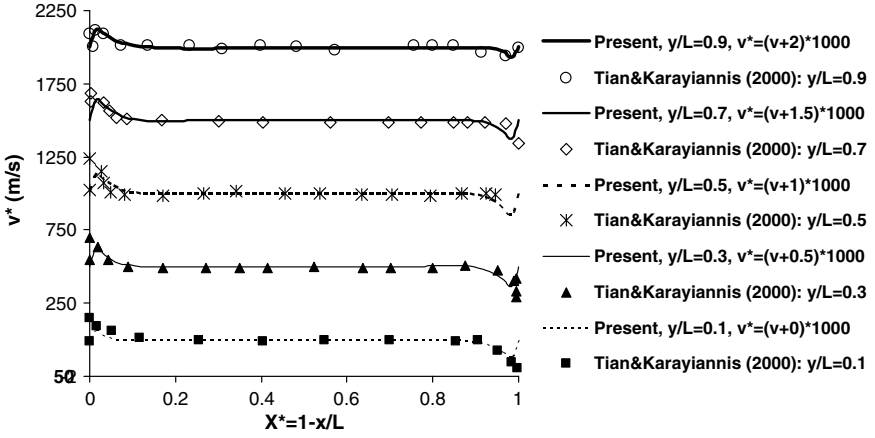

Fig. 7. Vertical velocity profiles between the hot and cold walls at various heights of the enclosure.

at $T_o = 293$ K, with the ground at the same constant temperature. Symmetry boundary conditions were applied in the spanwise and vertical direction and fully developed flow at the outlet. For the cube's solid walls, conjugate heat transfer boundary conditions are applied and the standard wall function approach is used for the momentum equations next to all solid boundaries.

Calculation of the flow past the hollow cube has been performed for three different external flow Reynolds numbers ($Re = U_0 H/\nu = 2 \times 10^5$, 5×10^5 and 1×10^6), two different heat flux values ($q = 20$ and 40 W m^{-2}) and four different outer face heat flux orientations (top, upstream, downstream and one of the side faces). The external heat flux values are rather low to correspond to solar heat gains, but the present calculation is performed at steady state so actual values would lead to unrealistic inner temperatures. The Reynolds numbers correspond to common wind velocity values of $U_0 = 1$, 2.5 and 5 m s^{-1}, respectively. The effect of the external Reynolds number and heat flux value is examined for the upstream and downstream heat flux orientations and the full effect of heat flux orientation as well as the relative influence of convective and radiative heat transfer is examined at $Re = 2 \times 10^5$ and $q = 20$ W m^{-2}. During calculations, it was found beneficial for convergence to calculate external flow while maintaining internal cube temperature constant and to subsequently introduce internal natural convection flow and then radiation effects. The grid size was the same for all calculations: $62 \times 50 \times 76$, with 30 points on the cube edges but calculations were also performed with an $82 \times 60 \times 91$ grid and 39 points on the cube edges for the downstream and top heat flux directions. Variations in the internal and external face mean temperatures were between 3% and 12% of the maximum temperature difference.

The Nusselt number is defined:

$$Nu = \frac{q \cdot H}{k_t \cdot (T_{sf} - T_o)} = \frac{(dT/dn) \cdot H}{(T_{sf} - T_o)} \tag{20}$$

where (dT/dn) is the temperature gradient normal to the surface, T_{sf} is the surface temperature and T_o is the upstream temperature. For the cube mean Nusselt number, the mean value of the five exposed faces is calculated. Surface cooling of a heated cube exposed to external flow has been studied in the past and external surface and cube mean Nusselt number correlations all agree to the form $Nu = c \cdot Re^n$ with $n < 1$ (see e.g. [2,3]).

Calculations were performed for a $q = 20$ W m^{-2} heat flux, initially on the upstream cube face and then on the downstream one, for Reynolds numbers in the range of $Re = 2 \times 10^5$–1×10^6 and the cube mean Nusselt number and air temperature are presented in Fig. 8. With increasing Reynolds number, the Nusselt number increases according to an $n = 0.60$ exponent (close to the $n = 0.68$ value found by Nakamura et al. [3]) and thus leads to an

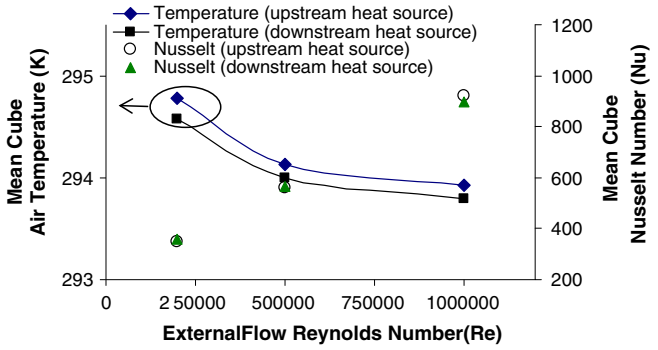

Fig. 8. Effect of flow Reynolds number on mean cube air temperature and mean cube Nusselt number.

asymptotic decrease in cube mean temperature. The opposite effect can be observed if, for comparison purposes, the heat flux is doubled to $q = 40\ \mathrm{W\ m^{-2}}$ at an external Reynolds number of $Re = 2 \times 10^5$. The resulting distribution of internal cube face temperatures is shown in Fig. 9 for the two cases of upstream and downstream orientation of external heat flux. Results for the lower

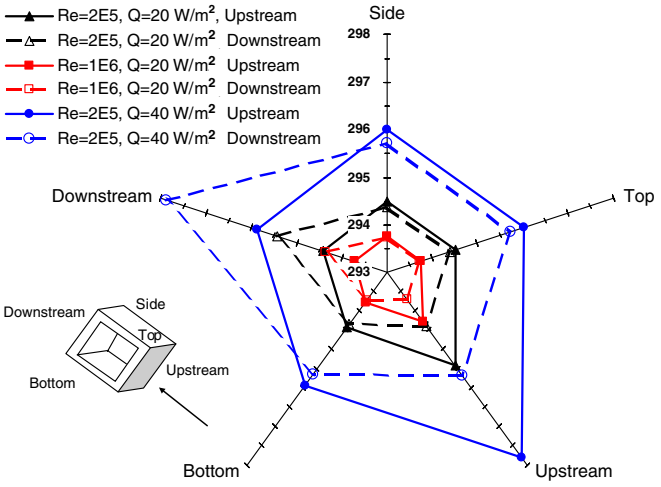

Fig. 9. Inner cube face temperatures for heat flux on upstream and downstream orientated external faces.

heat flux value ($q = 20\ \mathrm{W\ m^{-2}}$) at the same Reynolds number as well as a higher Reynolds number ($Re = 1 \times 10^6$) are also shown. The higher heat flux value leads to higher inner temperatures and the higher Reynolds number induces a stronger cooling effect but the relative spatial temperature distribution remains the same: when the upstream cube face is heated, the inner surface temperatures and the cube mean temperature are higher. The temperature difference between the hottest and coldest face is between 0.6 and 2 K for the cases presented in Fig. 9 but all Rayleigh number values are in the range $Ra = 1.5\text{–}5 \times 10^9$ i.e. above the turbulent threshold ($Ra > 10^8$).

The relative "asymmetry" between upstream and downstream heating is further demonstrated through Figs. 10 and 11. Fig. 10a shows the temperature distribution on the external surfaces of the cube when the upstream face is heated with a heat flux of $q = 20\ \mathrm{W\ m^{-2}}$ and the external flow Reynolds number is $Re = 2 \times 10^5$. Streaklines indicate the presence of the upstream stagnation zone and horseshoe vortex, as well as the recirculation zones on the top, side and downstream faces. The "hot spot" at the front stagnation region is prominent, as are the cooler edges, but the hot fluid captured within the top and side recirculation zones, combined with conduction through the envelope, leads to a temperature increase on the rest of the surfaces as well. Fig. 10b shows the corresponding buoyancy induced inner flow: the warmer upstream face causes a recirculation zone of air that rises, follows the ceiling and declines along the back but turns upward again midway along the bottom face. This is explained by the radiatively heated area near the front of the bottom face which lifts the flow before it reaches the upstream face. A radiatively heated region is also evident on the outer surface of the downstream face, which does not appear when radiation effects are not included. At the same Reynolds number ($Re = 2 \times 10^5$) but at double the heat flux value ($q = 40\ \mathrm{W\ m^{-2}}$) the surface temperatures and the temperature differences become larger leading to a doubling of Rayleigh number ($Ra = 4.5 \times 10^9$) and the recirculation zone is now pushed towards the top and downstream face (Fig. 11a). The asymmetry of the inner and outer flow and heat transfer for upstream and downstream heating is clear in Fig. 11 for the higher heat flux value. The cube's inner surface temperature range is roughly the same when upstream (Fig. 11a) and downstream faces (Fig. 11b) are heated but the variation in temperature difference induces a different inner flow, possibly due to the slightly higher inner surface temperature differences for downstream heating (see also Fig. 9): $Ra = 5 \times 10^9$ as opposed to $Ra = 4.5 \times 10^9$ for upstream heating. On the outer surfaces of the cube envelope, an iso-temperature

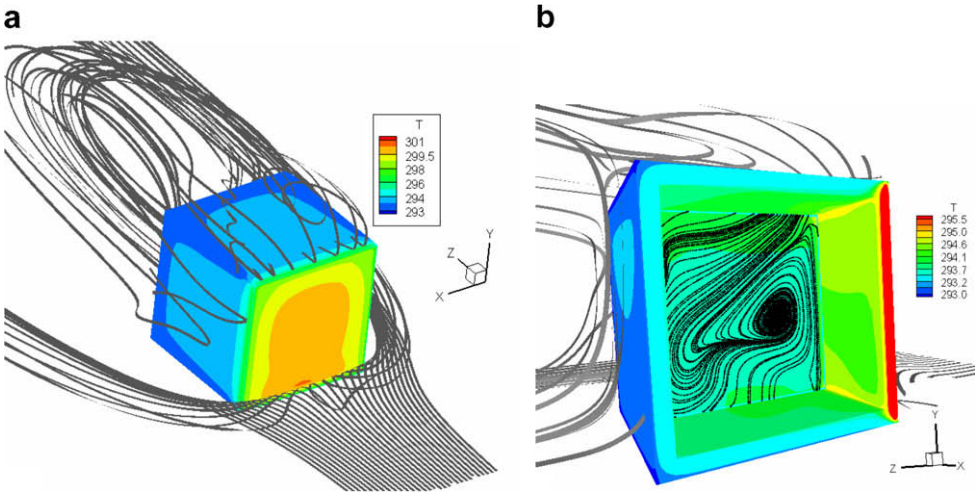

Fig. 10. Temperature and flow field (a) around and (b) inside cube envelope when heat flux is on upstream side ($Re = 2 \times 10^5$, $q = 20\ \mathrm{W\ m^{-2}}$).

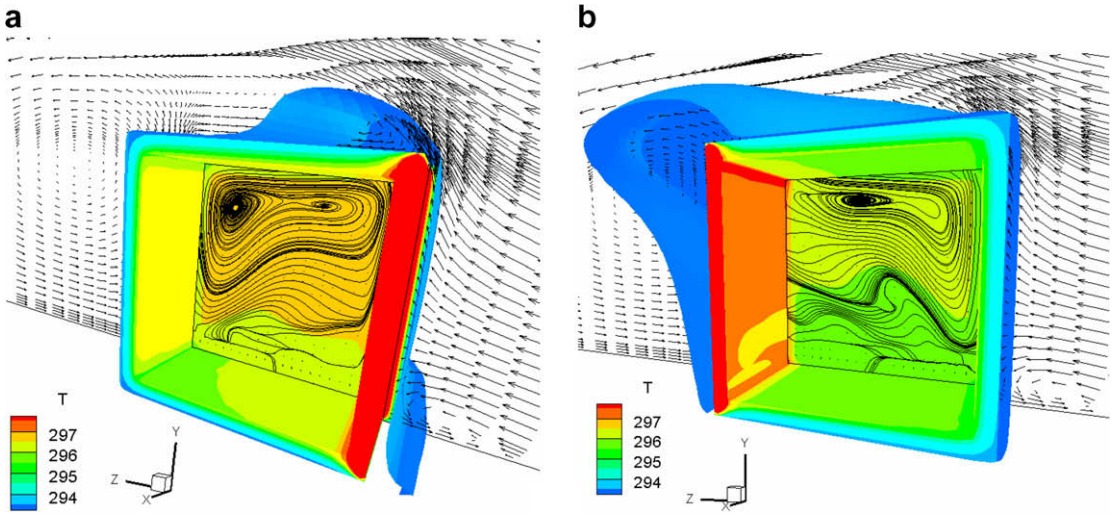

Fig. 11. Temperature and flow field in and around the cube envelope when heat flux is on (a) upstream and (b) downstream side. Streaklines have been projected onto the center-plane and the outer temperature iso-surface value is $T = 293.1$ K ($Re = 2 \times 10^5$, $q = 40$ W m^{-2}).

surface has been plotted at the value of $T = 293.1$ K. These zones are indicative of the heat dissipated by the flow and the extensive warm air zones in Fig. 11b show the heat leaving the cube. In Fig. 11a, these regions are thinner, implying that more heat is being transferred to the other cube faces, leading to higher surface temperatures.

The relative variation of mean temperature values and Nusselt numbers on the cube's external faces are presented in Table 1 and Table 2 for all possible heat flux orientations for $Re = 2 \times 10^5$ and $q = 20$ W m^{-2}. The temperatures of the cube faces show a minimal variation of $\Delta T = (T_{face} - T_o)$ while the heated face is 3–4 K hotter than the unheated faces for all cases. One would have expected a stronger dependence on orientation but this is actually more evident in the convective Nusselt numbers (Table 2). Comparison with the experimental correlation of Nakamura et al. [3] is also shown and should be compared with the heated face for each situation. Upstream and downstream values are in relatively good agreement with the correlations and, although the top and side values are appropriately predicted higher than the upstream and downstream ones, they are underestimated by about 30%, due to the turbulence modelling difficulties already discussed. On the other hand, this introduces a uniformity in the heat transfer among the cube surfaces that actually makes the present discussion conservative in its points and conclusions.

Calculation of the inner flow, induced by the non-uniform cooling of the envelope, has already been shown for upstream and downstream cooling. The situation with the heat flux on the top face is presented in Fig. 12 where the effects of convective and radiative heat transfer on the inside of the cube are evident. Fig. 12a shows the inner temperature distribution when the air is considered stagnant (i.e. only conductive heat transfer) while in Fig. 12b air motion induces convective effects and leads to a cooler ceiling but hotter side walls. The full effect of conduction, convection and radiation is presented in Fig. 12c where the induced flow ($V_{max} = 0.03$ m s^{-1}) and the higher temperatures on the floor and sidewalls are evident. The differences in the sidewall temperatures that are induced by the effect of the outer flow lead to a slight asymmetry with the center of the recirculation zone being pushed towards the downstream face.

The relative influence of convection and radiation on the inner temperature field is further demonstrated in Fig. 13 where the radial graphs have been plotted for the four different heating orientations and results are shown for stagnant air, pure convection and convection–radiation. Temperature differences of over 4 K arise when convection and radiation are taken into account instead of stagnant air, especially on the heated face. Even more interesting is the fact that thermal radiation leads to a more uniform internal temperature distribution among the surfaces whereas pure convection is not as effective in this regard. The heated surface remains at a much higher temperature without radiation effects, which tend to cool it and simultaneously heat the others, leading to the uniformity in temperature. This effect is a direct consequence of keeping the heat flux constant and letting conduction, convection and radiation determine the wall's temperature. In

Table 1
Mean temperatures on the outer faces of the cube, depending on the direction of the heat flux ($Re = 2 \times 10^5$, $q = 20$ W m^{-2})

Temperatures (K)	External heat source direction			
	Upstream	Downstream	Top	Side
Side	293.48	293.46	293.39	296.85
Top	293.44	293.43	296.73	293.40
Upstream	296.64	293.33	293.41	293.42
Downstream	293.35	297.03	293.43	293.41

Table 2
Mean Nusselt numbers on the outer faces of the cube, depending on the direction of the heat flux ($Re = 2 \times 10^5$, $q = 20$ W m^{-2})

Nu	External heat source direction				Correlations from [3]
	Upstream	Downstream	Top	Side	
Side	368.41	331.35	358.24	390.44	$\overline{Nu}_s = 0.12Re^{0.70} = 598$
Top	373.50	355.69	411.90	355.41	$\overline{Nu}_t = 0.071Re^{0.74} = 575$
Upstream	380.61	377.40	380.02	379.74	$\overline{Nu}_f = 0.71Re^{0.52} = 396$
Downstream	309.58	332.46	296.13	309.19	$\overline{Nu}_r = 0.11Re^{0.67} = 380$

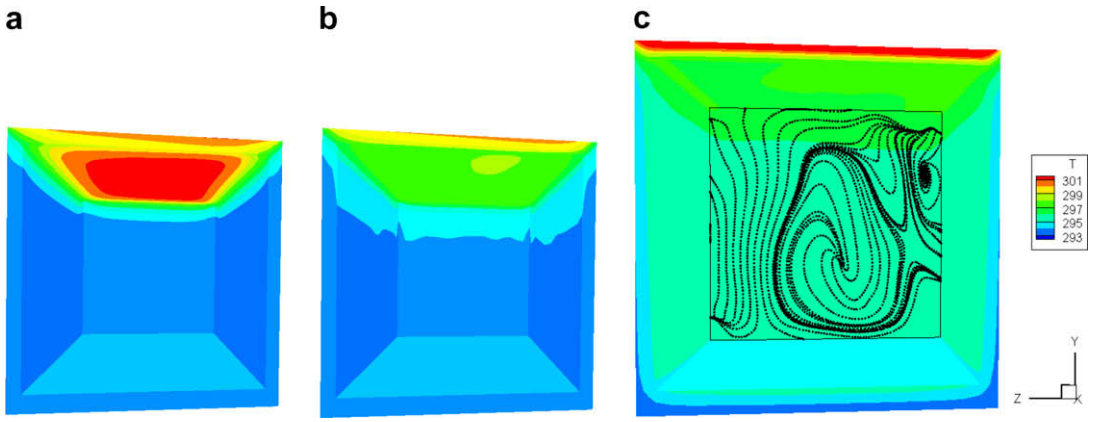

Fig. 12. Temperature distribution inside the cubicle considering (a) stagnant air without radiation effects, (b) natural convection without radiation effects, (c) natural convection including radiation effects ($Re = 2 \times 10^5$, $q = 20\ \mathrm{W\ m^{-2}}$).

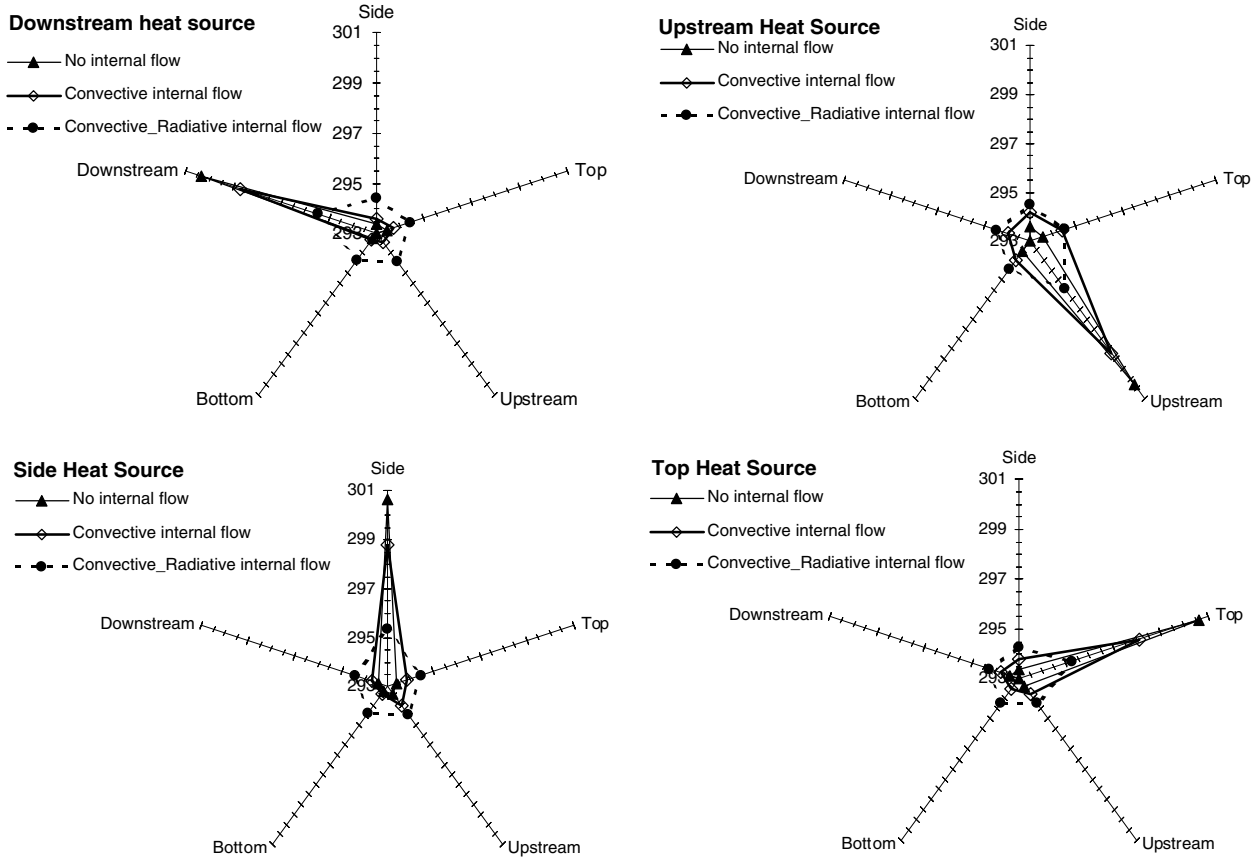

Fig. 13. Variation of the mean temperatures of the inner surfaces of the cube, depending on the effects of convection and radiation for: (a) downstream heat source; (b) upstream heat source; (c) side heat source; (d) top heat source ($Re = 2 \times 10^5$, $q = 20\ \mathrm{W\ m^{-2}}$).

situations where studies focus on constant temperature walls, such an effect cannot be observed.

The interaction of the outer flow and the orientation of the heated surface and their effect on the inner flow and temperature distributions can be seen more clearly in Fig. 14. For each of the four heat source orientations that were studied, the five surfaces' mean temperatures are plotted on the corresponding axis. The mean cube air temperature is also plotted on the axis that corresponds to the surface being heated. Here it can be seen that the inner temperature differences are not negligible (over 0.5 K) and that there is also a significant difference in the mean cube temperature, depending on the heat source orientation with regard to the external flow direction. The relative effects of upstream and downstream heating have already been discussed with regard to Fig. 11 and similar conclusions are drawn here, for the lower heat flux value. The highest temperatures, both the mean cube air and the inner surfaces, arise when the heat source is on the upstream side while heating on the top leads to the lowest inner temperatures. When the upstream face is heated, although the surface Nusselt number is low (see Table 2), the dissipated heat is transferred to the downstream surfaces, leading to their higher surface temperatures when compared to the other heating orientations (Table

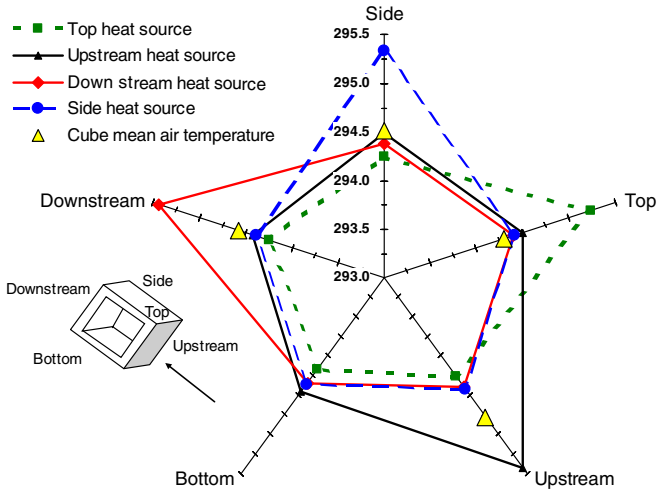

Fig. 14. Mean temperatures of the inner surfaces and the cube for the different heat source directions that were examined. The mean cube temperature for each heating orientation is placed on the radial axis that corresponds to the heated surface ($Re = 2 \times 10^5$, $q = 20\ \mathrm{W\ m^{-2}}$).

1). On the other hand, the higher Nusselt numbers on the heated top and side surfaces, which are already underpredicted (see Table 2), explain the lower temperatures inside the cube, especially since the heat is carried away by the flow. The large recirculation zone behind the cube leads to a low Nusselt number on the downstream heated face and the higher temperatures on the outer surface (Table 1) and the cube inner air temperature.

4. Conclusions

A study of combined fluid flow and heat transfer including forced and natural convection, thermal radiation and conduction through solid–fluid interfaces has been performed for the heat transfer through a cubic envelope subjected to external flow. The numerical methodology that has been implemented includes all heat transfer modes in an implicit solution procedure through a novel boundary condition at the solid–fluid interface for convection and thermal radiation effects.

The methodology was first validated by comparison to experimental and numerical results from the literature for laminar and turbulent natural convection in enclosures, with and without radiation and conjugate heat transfer effects. There are some simplifications applied, especially with regard to the turbulence modelling of the moderately turbulent ($Ra \sim 10^9$) buoyant flow in the cavity and the heat transfer on the outer cube surfaces. However, validation calculations show that the methodology can be used to derive qualitative conclusions with regard to a configuration that, to the authors' knowledge, has not been previously studied.

It has been shown that radiation effects between the inner surfaces of a cubic enclosure can play a significant role in determining the temperature distribution when a constant heat flux is the heat source. An increase in the Reynolds number of the external flow affects the cube Nusselt number and leads to an asymptotically decreasing mean cube temperature. Different heat flux values similarly increase the mean temperatures although both cooling due to higher Nusselt numbers and heating due to higher heat flux values seem to retain the inner surfaces' relative temperature distribution. The orientation of the heat source with regard to the external flow is also important. Due to the outer flow and buoyancy forces, a heat flux applied from different orientations will lead to different inner flow and temperature patterns. Heating on the upstream surface causes much of the heat to remain within the cube and leads to higher inner temperatures than for other heat source orientations.

Acknowledgements

The research is co-funded by the European Union – European Social Fund & Natural Resources – EPEAEK II and the Greek Ministry of Education and Religious Affairs under the Pithagoras II program.

References

[1] P. Linden, The fluid mechanics of natural ventilation, Annu. Rev. Fluid Mech. 31 (1999) 201–238.
[2] E. Meinders, K. Hanjalic, R. Martinuzzi, Experimental study of the local convective heat transfer from a wall mounted cube in turbulent channel flow, J. Heat Transfer 121 (1999) 564–573.
[3] H. Nakamura, T. Igarashi, T. Tsutsui, Local heat transfer around a wall-mounted cube in the turbulent boundary layer, Int. J. Heat Mass Transfer 44 (2001) 3385–3395.
[4] E. Meinders, K. Hanjalic, Experimental study of the convective heat transfer from in-line and staggered configurations of two wall-mounted cubes, Int. J. Heat Mass Transfer 45 (2002) 465–482.
[5] Y. Cheng, F.S. Lien, E. Yee, R. Sinclair, A comparison of large Eddy simulations with a standard k–e Reynolds-averaged Navier–Stokes model for the prediction of a fully developed turbulent flow over a matrix of cubes, J. Wind Eng. Ind. Aerodynam. 91 (2003) 1301–1328.
[6] M. Tsuchiya, S. Murakami, A. Mochida, K. Kondo, Y. Ishida, Development of a new k–ε model for flow and pressure fields around bluff body, J. Wind Eng. Ind. Aerodynam. 67 and 68 (1997) 169–182.
[7] G. Iaccarino, A. Ooi, P.A. Durbin, M. Behnia, Reynolds averaged simulation of unsteady separated flow, Int. J. Heat Fluid Flow 24 (2003) 147–156.
[8] W. Rodi, Comparison of LES and RANS calculations of the flow around bluff bodies, J. Wind Eng. Ind. Aerodynam. 69–71 (1997) 55–75.
[9] N.C. Markatos, M.R. Malin, G. Cox, Mathematical modelling of buoyancy-induced smoke flow in enclosures, Int. J. Heat Mass Transfer 25 (1) (1982) 63–75.
[10] E.M. Sparrow, J.P. Abraham, A new buoyancy model replacing the standard pseudo-density difference for internal natural convection in gases, Int. J. Heat Mass Transfer 46 (2003) 3583–3591.
[11] S. Bajorek, J. Lloyd, Experimental investigation of natural convection in partitioned enclosures, J. Heat Transfer 104 (1982) 527–532.
[12] E. Zimmerman, S. Acharya, Free convection heat transfer in a partially divided vertical enclosure with conducting end walls, Int. J. Heat Mass Transfer 30 (2) (1987) 319–331.
[13] Y. Tian, T. Karayiannis, Low turbulence natural convection in an air filled square cavity. Part I: the thermal and fluid flow fields, Int. J. Heat Mass Transfer 43 (2000) 849–866.
[14] H.S. Dol, K. Hanjalic, Computational study of turbulent natural convection in a side heated near cubic enclosure at a high Rayleigh number, Int. J. Heat Mass Transfer 44 (2001) 2323–2344.
[15] M. Kasemi, M. Naraghi, Analysis of radiation–natural convection interactions in 1-g and low-g environments using the discrete exchange factor method, Int J. Heat Mass Transfer 36 (17) (1993) 4141–4149.
[16] A. Mezrhab, H. Bouali, H. Amaoui, M. Bouzidi, Computation of combined natural-convection and radiation heat-transfer in a cavity having a square body at its center, Appl. Energ. 83 (2006) 1004–1023.
[17] V. Dharma Rao, S.V. Naidu, B. Govinda Rao, K.V. Sharma, Heat transfer from a horizontal fin array by natural convection and radiation – a conjugate analysis, Int. J. Heat Mass Transfer 49 (2006) 3379–3391.
[18] A.K. Sharma, K. Velusamy, C. Balaji, S.P. Venkateshan, Conjugate turbulent natural convection with surface radiation in air filled rectangular enclosures, Int J. Heat Mass Transfer 50 (2007) 625–639.
[19] J.L. Consalvi, B. Porterie, J.C. Loraud, Method for computing the interaction of fire environment and internal solid regions, Numer. Heat Transfer, Part A 43 (2003) 777–805.
[20] X. Chen, P. Han, A note on the solution of conjugate heat transfer problems using SIMPLE-like algorithms, Int. J. Heat Fluid Flow 21 (2000) 463–467.
[21] D. Bouris, A 3D calculation of the flow and heat transfer in and around a hollow cubicle exposed to external flow, in: 1st International Conference "From Scientific Computing to Computational Engineering", 1st IC-SCCE, Athens, 8–10 September, 2004.
[22] M. Petridou, D. Bouris, Experimental and numerical study of the effect of openings on the surface pressure distribution of a hollow cube, WSEAS Trans. Fluid Mech., 1790-5087 1 (6) (2006) 655.
[23] S. Patankar, D. Spalding, A calculation procedure for heat mass and momentum transfer in three dimensional parabolic flows, Int. J. Heat Mass Transfer 15 (1972) 1787.
[24] C. Rhie, W. Chow, Numerical study of the turbulent flow past an airfoil with trailing edge separation, AIAA J. 21 (1983) 1525–1532.
[25] B.E. Launder, D.B. Spalding, The numerical computation of turbulent flows, Comput. Methods Appl. Mech. Eng. 3 (1974) 537.

[26] D.B. Spalding, Contribution to the theory of heat transfer across a turbulent boundary layer, Int. J. Heat Mass Transfer 7 (3) (1964) 743–761.
[27] C.L.V. Jayatilaka, The influence of Prandtl number and surface roughness on the resistance of laminar sublayers to momentum and heat transfer, Prog. Heat Mass Transfer 1 (1969) 193–329.
[28] H.B. Awbi, Calculation of convective heat transfer coefficients of room surfaces for natural convection, Energ. Build. 28 (1998) 219–227.
[29] G. Papadakis, G. Bergeles, A locally modified second order upwind scheme for convection terms discretisation, Int. J. Numer. Methods Heat Fluid Flow 5 (1995) 49–62.
[30] J.A. Clarke, Energy Simulation in Building Design, second ed., Butterworth, Heinemann, 2001.
[31] J.R. Howell, A Catalog of Radiation Heat Transfer Configuration Factors, University of Texas, Austin second ed., 2001, Available online at: <http://www.me.utexas.edu/>.
[32] D. Bouris, G. Bergeles, Numerical calculation of the effect of deposit formation on heat exchanger efficiency, Int. J. Heat Mass Transfer 40 (17) (1997) 4073–4084.
[33] X. Li, P. Durbetaki, The conjugate formulation of a radiation induced transient natural convection boundary layer, Int. J. Numer. Methods Eng. 35 (1992) 853–870.